Journal of Chemical Physics, 2006, vol. 125, no. 23, p. 234701.

Spectra of the liquid cluster surface thermal fluctuations

D. I. Zhukhovitskii*
Institute of High Temperatures, Russian Academy of Sciences, Izhorskaya 13/19, 125412 Moscow, Russia
(Dated: October 26, 2006)

Classification of cluster particles is proposed that introduces three particle types: the internal particles, surface particles, and virtual chains of particles. Thermal fluctuations of a surface passing through the surface particles of a Lennard-Jones liquid cluster are studied using a molecular dynamics simulation. It is shown that for large clusters, the Fourier spectral amplitude of these fluctuations decays faster than $1/q$, where q is the wave number. The frequency Fourier spectrum shows an overdamped system behavior, which is the evidence for the absence of thermal capillary waves for clusters comprising $\lesssim 10^5$ particles. The time-averaged cluster density profile is given by an error function with the width parameter diverging as the logarithm of the cluster size.

PACS numbers: 68.10.-m, 68.10.Cr, 68.10.Et

I. INTRODUCTION

The fine structure of liquid–vapor interface has been widely discussed since Gibbs's fundamental works[1]. Studying the interface is a source of information concerning its energy characteristics, which are input parameters in the kinetics of the first-order phase transition[2,3]. Gibbs introduced a thin interface layer dividing two phases. This layer is subject to thermal fluctuations, which are investigated by various approaches. One approach proposed by Buff, Lovett, and Stillinger[4] treated the fluctuations as capillary waves that were thermally excited on a model zero-width elastic surface, which represented the interface. The fluctuation Fourier spectrum was calculated with the an allowance made for gravitation. The interfacial width was found to diverge logarithmically as the force of gravity tended to zero. This approach was developed in Refs.[5–7], where such effects as the nonzero intrinsic width of the interface[5], surface tension renormalization[6], and coupling of thermal modes[7] were included. The fluctuation spectrum of the spherical cluster surface calculated in Ref.[8] by expansion in spherical harmonics $Y_{lm}(\Omega)$ rapidly approaches that of a flat surface as l tends to infinity. The density functional approach for a curved interfacial layer was proposed by Fisk and Widom[9]. The effective Hamiltonian used in Ref.[10], which is a nonlocal and a nonbilinear function of the interface configuration, leads to a divergence of the curvature coefficient for the power particle interaction potentials. The Hamiltonian leads to divergence-free expressions if the intrinsic structure of the interface with finite width is included[11].

Fluctuations of the liquid–vapor interface were studied experimentally by x-ray reflectivity measurements at the interface of normal alkanes[12]. Freezing of the capillary waves on glycerol surfaces was observed by means of x-ray photon correlation spectroscopy[13]; the transition from propagating to overdamped dynamic behavior of capillary waves for the water/glycerol mixture was observed in Ref.[14]. By means of x-ray diffuse scattering, it was demonstrated that a bimolecular layer drastically enhances capillary wave fluctuations on the water surface[15]. Fluctuations at the interface between two fluid phases show qualitatively the same regularities as those at the free interface[16,17].

The dependence of interface width on the surface area of a liquid–vapor boundary was studied by molecular dynamics (MD) simulation in Ref.[18]. Up to temperatures close to the critical one the interface width estimated in this study proved to be a linear function of $\ln A$, where A is the interface surface area. In order to fit the temperature dependence of the interface width, the internal interface width was used as an adjustable parameter. Similar results were obtained in MD simulation of the water surface[19].

In all experimental studies, as well as in MD simulation, solely the integral interface characteristic (width parameter) was estimated. This quantity is insufficient to establish the relevance of various theories of capillary wave fluctuations, so more detailed information, namely the fluctuation spectra, are necessary. Information of this kind is absent in the literature because the definition of a fluctuating surface that would represent the instantaneous position of the free liquid–vapor interface is lacking. Such a definition is proposed and used in this work. We start from the assumption that at every instant the cluster interface has no internal structure, and the density changes abruptly from liquid to vapor; an instantaneous geometrical configuration of the interface can be essentially nonspherical. In other words, the average distance between particles is assumed to be independent of their positions in the cluster up to the interface, and the fluctuating surface can be identified with a surface passing through some monolayer particles that mark the cluster boundary. By definition, cluster particles are divided in three groups. The internal particles constitute the cluster core and are assumed to have the same properties. A definition of surface particles weakly dependent on the surface local curvature is proposed, which implies that these particles are situated on top of the internal ones. The third group includes fluctuation overhangs or the groups of particles with a minimum number of bonds anchored to the surface (virtual chains).

This particle classification can be used in a MD simu-

lation, which was performed for clusters. A cluster is an object that makes it possible to estimate both the curvature dependence of the investigated properties and their limiting values as the cluster size tends to infinity, i.e., for a planar interface. The (P, T)-ensemble method[20] was chosen as the basic simulation algorithm because it is free from possible effects of microcanonical ensemble simulation such as the size finiteness, energy conservation, and periodic boundary conditions. The selected method implies the simulation of a single cluster of variable size placed in the vapor environment, which is the Maxwell weakly nonideal gas. This gas is generated in a sufficiently large "transparent" cell by a special procedure that conserves neither the number of particles nor the energy of the system. The cluster can grow, decrease in size, or find itself in the state of unstable equilibrium with the surrounding vapor, as in the case of a real system. The data obtained from the MD simulation are used in the Fourier analysis of the configurations of the cluster surface, both in the wave number and frequency spaces.

The paper is organized as follows. In Sec. II, the MD simulation procedure is discussed, and in Sec. III, cluster particles are divided in three groups and the cluster surface is defined. Spectra obtained on the basis of this definition are discussed and compared with the theory in Secs. IV and V for the wave number and frequency spectrum, respectively. The average interfacial density profile is discussed in Sec. VI. The results of this paper are summarized in Sec. VII.

II. SIMULATION PROCEDURE

We use the MD simulation method that mimics real conditions of vapor nucleation, the (P, T) ensemble[20]. The cluster finds itself close to the center of a spherical cell. The cell surface generates vapor particles with the Maxwell distribution over velocities. The particles that reach the surface from inside are removed from the simulated system. If the cell radius R_c is sufficiently larger than the cluster radius R, the Maxwell vapor particles distribution with a time-independent density n_v and temperature T is established in the cell. The (P, T)-ensemble simulation begins with construction of a cluster in the center of a cell. Then the vapor generation procedure starts, and upon some time, the process becomes quasistationary.

The system particles interact via the widely used Lennard-Jones potential

$$u(r) = \begin{cases} v(r) - v(r_c), & r \le r_c, \\ 0, & r > r_c, \end{cases} \qquad v(r) = 4\varepsilon \left(\frac{a^{12}}{r^{12}} - \frac{a^6}{r^6} \right), \tag{1}$$

where r is the interparticle distance; $r_c = 2.5a$ is the cutoff radius; ε is the well depth; and a is the length scale. The carrier gas is included in the simulation as the Berendsen thermostat in the way it was done in Ref.[20]. In what follows, we use the following MD units: $\tau_0 = a\sqrt{M/24\varepsilon}$ for the time (M is the particle mass); a for the distance; a^{-3} for the particle density; ε for the energy; ε/a^2 for the surface tension. Also, we use the energy units for temperature T, i.e., the Boltzmann constant is set to unity.

Simulations were performed for three temperatures, $T = 0.603$, 0.67, and 0.75; the vapor densities were $n_v = 0.0028$, 0.0058, and 0.012, respectively. The initial cluster size was $g = 3500$ at the cell radius $R_c = 16$. According to Ref.[21] even at $T = 0.603$, the clusters with $g < 3500$ are in the liquid state. At selected vapor densities, which were somewhat lower than the equilibrium ones for the Lennard-Jones system with a flat liquid–vapor interface[22], the cluster evaporated slowly until it disappeared; then a new run began with the same initial cluster size. The total time of cluster evolution was 135000, during which 18 clusters evaporated completely.

According to the classical nucleation theory[3], in the case of supersaturated vapor, the cluster with size larger than the critical one g^* increases in size; at $g < g^*$, the cluster evaporates. The supersaturation ratio $S_v = n_v/n_s$, where n_s is the saturated vapor density, is related to g^* as $\ln^3 S_v = 32\pi\gamma^3/n_\ell^2 T^3 g^*$, where γ is the surface tension for a flat interface; and n_ℓ is the density of bulk liquid. For $T = 0.75$, $g^* = 3500$, and the values $\gamma(0.75) = 0.483$, $n_\ell = 0.762$, characteristic of interaction potential (1), we have $S_v = 1.27$. Therefore, $n_v \simeq n_s$, and for the conditions specified above, clusters are in the state not far from equilibrium.

To improve the statistics at small g, an additional series of runs was performed at the initial cluster size $g = 400$ ($T = 0.75$; $R_c = 8$; the total evolution time was 253000). The region of large sizes was investigated by simulation of a cluster with the size decreasing from $g = 30000$ down to 20000 ($T = 0.75$; $R_c = 35$; evolutions of two clusters were observed). After the relaxation time (200, 600, and 2000 for initial sizes of 400, 3500, and 30000, respectively), coordinates of all system particles were recorded in time intervals of 25 and stored for subsequent processing. During processing the quantities under investigation were averaged over all runs and cluster sizes ranging from $0.9g$ to $1.1g$ and then assigned to the size g.

III. DEFINITION OF CLUSTER SURFACE

To distinguish between the particles that comprise a cluster and vapor we use the Stillinger definition[23], according to which a particle belongs to the cluster if it has at least one neighbor particle at the distance less than r_b, which belongs to this cluster. Thus, g is a function of r_b. However, for sufficiently large clusters, there exists such a value of this quantity at which $dg/dr_b = d^2g/dr_b^2 = 0$; that is, in the vicinity of this value, g is independent of

r_b[24]. For $T = 0.603$, 0.67, and 0.75, $r_b = 1.59$, 1.62, and 1.65, respectively; these values are close to the coordinates of first minima of the radial distribution function in large clusters[25] and are therefore proportional to $n_\ell^{-1/3}$. At the same time, r_b defines the equimolar cluster radius $R = r_\ell g^{1/3}$, where $r_\ell = (3/4\pi n_\ell)^{1/3}$. Along with this cluster size definition, we will use the definition of a bond. A particle will be assumed to have b bonds if b neighbor particles are situated at a distance not exceeding r_b from the particle, i.e., b is the number of nearest neighbors.

Now we introduce a key definition that divides cluster particles into three groups. Assume that the origin of a coordinate system is situated at the cluster center of mass. Particle 1 with the radius vector $\mathbf{r}_1$ that belongs to the cluster will be called *internal* if there exists at least one particle 2 with radius vector $\mathbf{r}_2$ belonging to the same cluster that forms more than four bonds such that the conditions

$$\mathbf{r}_1 \cdot \mathbf{r}_2 > r_1^2, \quad r_2^2 - \frac{(\mathbf{r}_1 \cdot \mathbf{r}_2)^2}{r_1^2} < \frac{1}{3n_\ell^{2/3}} \qquad (2)$$

are satisfied. The cluster particles that are not internal and form more than four bonds will be called *surface* particles. By definition, the cluster particles that are not internal and form less than five bonds are *virtual chains*. They are anchored to the surface of the cluster, i.e., virtual chains are overhangs.

The first condition (2) means that particle 2 finds itself on top of particle 1, and, according to the second condition (2), it may not form a bond with particle 1 but must lie within some solid angle with a vertex at the center of mass of the cluster and an axis passing through particle 1. The left-hand side of the second condition (2) is the squared distance between particle 2 and this axis. The squared distance scale $1/3n_\ell^{2/3}$ on the right-hand side of this condition corresponds to the model concept according to which a surface particle is situated in a vertex of a regular tetrahedron with an edge length $n_\ell^{-1/3}$ equal to the mean distance between particles in the liquid, whereas the other particles that occupy the remaining tetrahedron vertices are internal. Since the average interparticle distance is assumed to be almost the same for all types of particles, the form of dependence of the length scale on particle density is obvious. The factor 1/3, which arises from the model discussed above, is also the best value, at which the monolayer of surface particles is clearly seen (Fig. 1), and the representation of particle distribution over the number of bonds in the form of two Gaussian exponents is most exact[24]. Note that the distance $1/\sqrt{3}n_\ell^{1/3} \simeq 0.632$ ($T = 0.75$) is almost half as large as the position of first maximum of the radial distribution function in a cluster[25], and the probability to find two particles at such small distance is very low. Conditions (2) assume that the angle between the normal to the surface and radius vector $\mathbf{r}_1$ is not too large; this is the case in the MD simulations discussed. These conditions are effective if the cluster surface is nonspherical due to fluctuations, and the simplest condition $r_2 > r_1$ is insufficient.

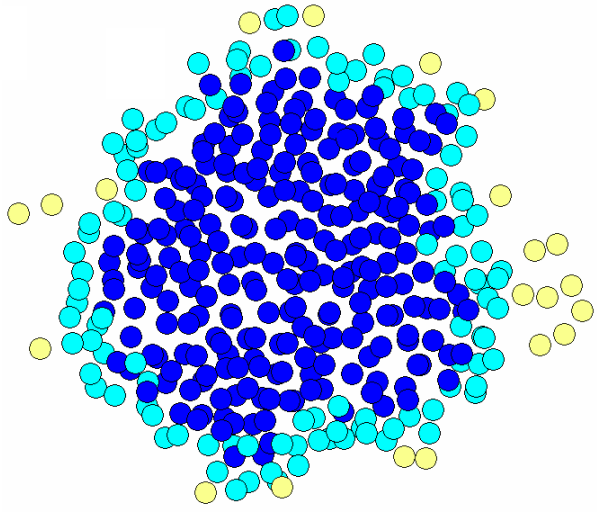

FIG. 1: Snapshot of cluster cross section at $g = 1592$, $T = 0.75$. Blue circles are internal particles, cyan circles are surface particles, and light yellow circles are virtual chains; vapor particles are not shown.

The definition introduced above becomes apparent in MD simulation. Figure 1 shows a typical snapshot of cluster particles situated between two parallel planes at a distance $h = 2.59$ between each other and $h/2$ from the cluster center of mass (here, $n_\ell^{-1/3} = 1.1$). Figure shows that the surface particles form a strongly curved monolayer on the bulk of internal particles. Also seen is the chainlike structure of overhangs (open circles).

To test definition (2), the distribution function of cluster particles over the number of bonds, which is equal to the mean number of particles with given number of bonds, was calculated. This distribution proved to be bimodal and was represented by the sum of two Gaussian exponents[24]. Each Gaussian exponent describes with good accuracy individual distributions for internal particles and surface particles plus virtual chains. Moreover, the distribution over a number of bonds for the particle closest to the center of mass normalized to the number of internal particles almost coincides with the distribution for all internal particles. Therefore, they occupy the same microscopic state that is entirely different from the state of surface particles.

Projections of the radial distribution function on the interfacial plane were measured in the MD simulation[26]. The peaks of projections are independent of the distance from the equimolar plane. This means that the average distance from a particle to its nearest neighbors is the same for all types of cluster particles. The average number of bonds for surface particles is lowered by the fact that they have no neighbors from the vapor side.

By definition, a particle in virtual chains has a low number of nearest neighbors and, consequently, a low

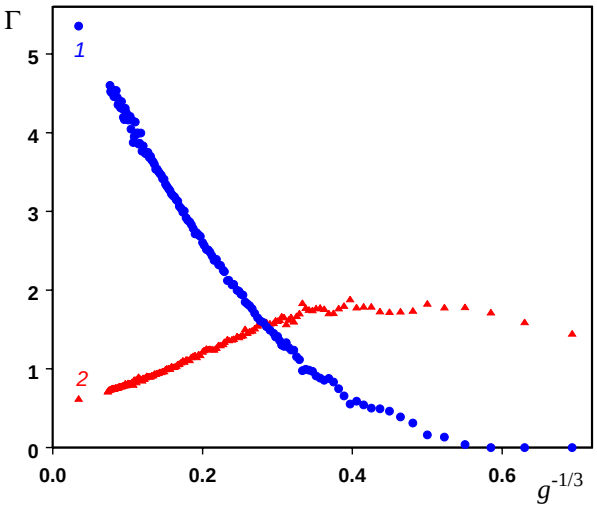

FIG. 2: Number of particles on the surface of a cluster as a function of its size at $T = 0.75$: $\Gamma = g_s g^{-2/3}$ [(1), the number of surface particles] and $g_{vc} g^{-2/3}$ [(2), the number of particles in virtual chains].

binding energy. One can expect that virtual chains play a principal role in evaporation. Monitoring all evaporation events at the cluster surface made it possible to calculate the distribution over the number of bonds for particles bonded with an evaporating particle[24]. This distribution contains a singularity at the point where the number of bonds is equal to two. In the vicinity of this point, the normalized distribution almost coincides with that for the cluster comprising four particles, whose typical configuration is a virtual chain[25]. This circumstance leads us to conclude that the characteristic number of particles in a virtual chain anchored to the cluster surface is of the order of four. The number of bonds for virtual chain particles was therefore limited to four, as suggested above. The presence of particles with more than two bonds takes into account both the existence of branching points and admixtures of compact states with the number of bonds greater than its minimum value[25].

The MD simulation data[24] lead us to the following model. The cluster is a homogeneous bulk of liquid with a nonspherical boundary perturbed by thermal fluctuations. Thus, the particle density experiences a jump at this boundary from the bulk liquid to vapor value. This allows us to formulate a definition of the *cluster instantaneous surface* as a surface passing through the surface particles.

Since the surface particles prove to be of special interest, we investigated the size dependence of their average number g_s (Fig. 2). For large clusters, the product $g_s g^{-2/3}$ increases linearly as $g^{-1/3}$ decreases until the asymptotic value of 5.97 is reached. For a planar interface, the surface particle density can be estimated as $\lim\limits_{g\to\infty} (g_s/A) = \lim\limits_{g\to\infty} [g_s/(4\pi r_\ell^2 g^{2/3})] \simeq 1.03$, i.e., approximately a single particle per the surface area a^2. The product $g_{vc} g^{-2/3}$, where g_{vc} is the average number of particles in virtual chains, increases linearly with $g^{-1/3}$ until $g^{-1/3} \simeq 0.34$. At $g < 6$, clusters comprise no surface particles and according to definition (2) no internal particles; they are merely virtual chains investigated in Ref.[25].

IV. WAVE-NUMBER FOURIER SPECTRUM OF SURFACE FLUCTUATIONS

As has been shown in the previous section, the cluster instantaneous density profile is abrupt; the boundary between liquid and vapor particles is marked by the surface particles. In this study, we will confine ourselves to a one-dimensional spectral analysis, which requires a much smaller array of simulation data than a two-dimensional analysis but still yields useful information. We will analyze the form of the boundaries of cross sections passing through a cluster center of mass. We will use samples of cluster particles situated between two parallel planes spaced by the distance h (Fig. 1) and isolate only the surface particles.

Consider a cross section layer with the width h perpendicular to the Z-axis of the Cartesian coordinate system with its origin in the cluster center of mass. We isolate g_{cs} surface particles that fall into this layer, whose coordinates z_j satisfy the condition $|z_j| \le h/2$, and define a function $P(\varphi_j)$ on the analytical grid $\varphi_j = 2\pi j/(2k_{\max}+1)$, where $0 \le j \le 2k_{\max}$, $k_{\max} = 0.9 g_{cs}$ is the maximum mode number. If the angle between the radius vector of the i-th surface particle $\mathbf{r}_i$ and X-axis, $\arccos(x_i/r_i)$ if $y_i \ge 0$ and $2\pi - \arccos(x_i/r_i)$ if $y_i < 0$, is next to φ_j then by definition $P(\varphi_j) = r_i$. This function defines the form of the cross-section boundary in the polar coordinates (P, φ) in the XY plane. Parameters of this definition ensure that the probability for two surface particles to fall in a single grid step is low. At the same time, the fraction of "empty" grid steps is not high.

Since $P(\varphi)$ has a period of 2π, it can be expanded in the Fourier series

$$P(\varphi) = \frac{\alpha_0}{2} + \sum_{k=1}^{k_{\max}} \alpha_k \cos k\varphi + \sum_{k=1}^{k_{\max}} \beta_k \sin k\varphi. \qquad (3)$$

The definition of $P(\varphi_j)$ and its approximation by (3) is illustrated in Fig. 3. Since the cluster is isotropic, it is necessary to average the spectral amplitudes $\alpha_k^2 + \beta_k^2$ over all Euler angles. Because $\alpha_k^2 + \beta_k^2$ is invariant relative to the rotation around the Z-axis, it is sufficient to consider the rotations around the X and Y axes characterized by the angles ψ_1 and ψ_2, respectively. Upon the rotation, coordinates of the i-th particle are transformed as follows:

$$\begin{pmatrix} x_i' \\ y_i' \\ z_i' \end{pmatrix} = E_2 E_1 \begin{pmatrix} x_i \\ y_i \\ z_i \end{pmatrix}, \quad E_1 = \begin{pmatrix} 1 & 0 & 0 \\ 0 & \cos\psi_1 & -\sin\psi_1 \\ 0 & \sin\psi_1 & \cos\psi_1 \end{pmatrix},$$

$$E_2 = \begin{pmatrix} \cos\psi_2 & 0 & -\sin\psi_2 \\ 0 & 1 & 0 \\ \sin\psi_2 & 0 & \cos\psi_2 \end{pmatrix}.$$

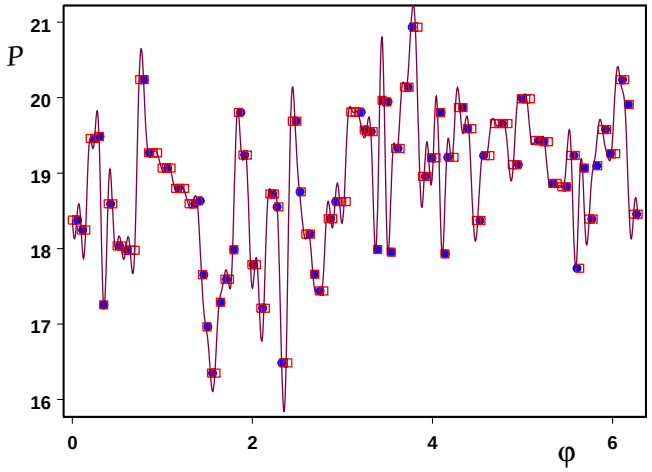

FIG. 3: Typical form of the cluster cross-section boundary for $g = 27395$, $g_s = 70$, $T = 0.75$. Distances of the surface particles from the cluster center of mass as functions of the polar angle in the cross-section plane (solid circles), function $P(\varphi_j)$ defined on the analytical grid (open squares), and its approximation by the Fourier series (3) (line).

The resulting average spectral amplitude S_k is defined as the weighted average over all combinations of rotation angles $\psi_1 = \pi m_1/20$ and $\psi_2 = \pi m_2/20$, $1 \le m_1, m_2 \le 40$,

$$S_k = \frac{\sum g_{cs} \left\langle \alpha_k^2 + \beta_k^2 \right\rangle_{\psi_1,\psi_2}}{\sum g_{cs}}, \qquad (4)$$

where the sums in (4) run over all cluster sizes from $0.9g$ to $1.1g$.

Obviously, S_k depends on the cross-section layer width h, whose value should be selected from compromise considerations. As h increases, cross sections overlap and phase interference leads to the decrease of spectral amplitudes (in Fig. 1, this is the case). As h decreases, the statistics becomes low and $k_{\max}$ decreases due to the decrease of g_{cs}. At optimum h, the average distance between particles in the cross section layer must be of the order of $n_\ell^{-1/3}$. Test calculations showed that the optimum is reached at $h = 1/\sqrt{3} n_\ell^{1/3}$, which is the smallest length scale of this problem appearing on the right-hand side of the second condition (2). We will use this scale in the following. It makes it possible to estimate the average number of surface particles in a cross-section $\bar{g}_{cs}$: if $h \ll R$ then $\bar{g}_{cs} \simeq 2\pi R h g_s/4\pi R^2 = \Gamma h g^{1/3}/2r_\ell$, where $\Gamma = g_s g^{-2/3}$.

Average spectral amplitudes (4) were calculated numerically for cluster configurations stored during MD simulation at $T = 0.75$ for different cluster sizes as functions of the mode number k. Figure 4(a) shows that S_k vanishes sharply at large k because the shortest wavelength cannot be shorter than the mean interparticle distance. The largest k corresponds to the wavelength of the order of $n_\ell^{-1/3}$. Since g_{cs} and therefore $k_{\max}$ differ

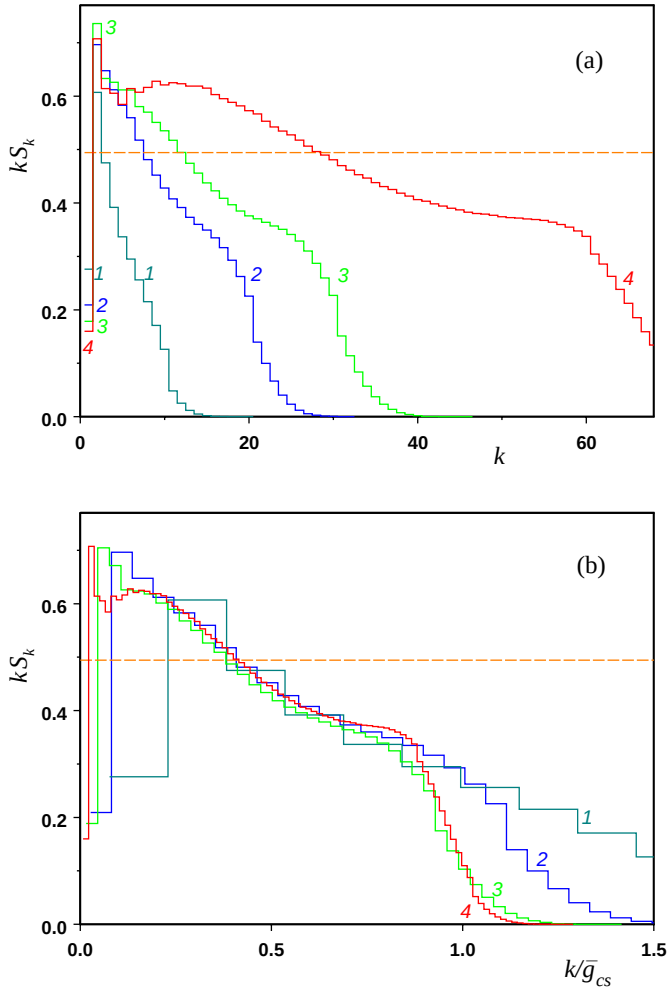

FIG. 4: Spectral amplitudes as a function of the mode number (a) and reduced mode number (b) for cluster sizes $g = 150$ (1), 1000 (2), 3000 (3), and 24450 (4); the dashed line represents theoretical estimate (9).

for different clusters, cluster surface configurations, and Euler angles, averaging (4) results in the diffuse right edge of S_k. At $k = 1$, S_k is low. Due to the momentum conservation, surface fluctuations proportional to spherical harmonics $Y_{lm}(\Omega)$ are impossible at $l = 1$. However, the spectra of angle-averaged cross sections of harmonics with $l > 1$ include the admixture of spectral amplitudes corresponding to $k = 1$. As is seen in Fig. 4(a), this admixture is rather moderate; it decreases with increasing cluster size. Obviously, spectral amplitudes decay faster than $1/k$.

If we plot kS_k as a function of $k/\bar{g}_{cs}$ for different g, then the curves almost coincide in the entire range of abscissa variation but the vicinities of $k \sim 1$ and $k \sim k_{\max}$ [Fig. 4(b)]. On the main segment, the spectra demonstrate a universal behavior (for given temperature), and

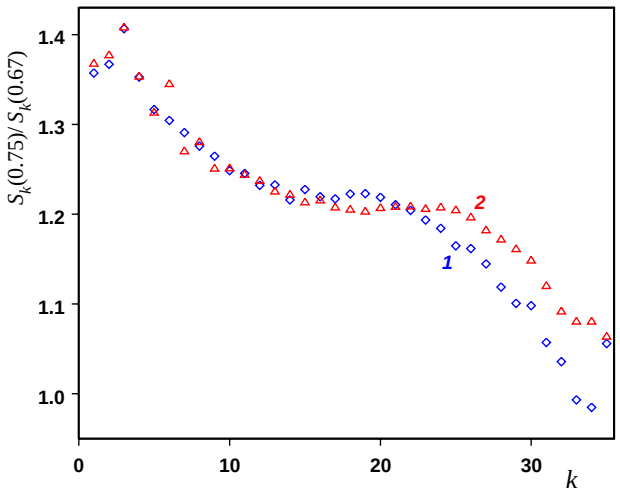

FIG. 5: Ratio of spectral amplitudes at different temperatures for $g = 2000$ (1) and 3000 (2).

kS_k can be approximated by a linear function

$$S_k = \begin{cases} \dfrac{0.731}{k} - \dfrac{0.572}{\bar{g}_{cs}}, & 2 \le k \le k_\infty, \\ 0, & k < 2 \text{ or } k > k_\infty, \end{cases} \tag{5}$$

where $k_\infty = 1.28\bar{g}_{cs}$ satisfies the condition $S_k(k_\infty) = 0$. As is seen from Eq. (5), the effect of surface curvature on S_k arises solely from the size dependence of Γ shown in Fig. 2. One could therefore expect that scaled spectral amplitudes (5) were the same for a planar interface ($g \to \infty$).

The ratio of spectral amplitudes calculated for $T = 0.75$ and 0.67 demonstrates that at small k the temperature dependence of S_k is noticeable, while at maximum k corresponding to amplitude vanishing, the ratio tends to 1, i.e., S_k is almost temperature independent (Fig. 5). Since cluster radii $R \sim 10$, and the size correction to surface tension must be negligibly small, the size correction cannot be responsible for such a behavior of $S_k(0.75)/S_k(0.67)$. Note that this ratio decreases with the increase of k even at small k, thus indicating the importance of the above-mentioned effect.

Now we give some theoretical estimates for the simplest case of a planar liquid–vapor interface, which has the form of a square with the side L. According to the fluctuation theory, the fluctuation probability is proportional to $\exp(-\Phi/T)$, where Φ is the minimum work of reversible fluctuation formation. At constant temperature, pressure, and cluster size, Φ has the same form as the capillary wave Hamiltonian (cf., e.g., Ref.[18])

$$\Phi = \gamma \Delta A = \frac{\gamma}{2} \int\limits_A dx\, dy\, |\nabla \xi(x,\, y)|^2, \tag{6}$$

where ΔA is the excess surface created by fluctuations; $\xi(x,\, y)$ is the position of fluctuation surface in the Z-axis perpendicular to the liquid–vapor interface; the origin of the Cartesian coordinate system is situated at a point where $\int\limits_A dx\, dy\, \xi(x,\, y) = 0$; integrals are taken over the entire surface area A. Upon substitution of the Fourier expansion $\xi(x,\, y) = \sum\limits_{\mathbf{q}} a_{\mathbf{q}} e^{i\,\mathbf{qr}}$ in (6), where $\mathbf{r} = \{x;\, y\}$ and $\mathbf{q} = \{2\pi n/L;\, 2\pi m/L\}$ are the two-dimensional radius vector and wave vector, respectively, $-N_{\max} \le n,\, m \le N_{\max}$ are integers, $N_{\max}$ is the maximum number of fluctuation modes in the X or Y axes, and $a_{\mathbf{q}=0} = 0$, one obtains

$$\Phi = \sum_{n,\, m} \tilde{\Phi}_{nm}, \quad \tilde{\Phi}_{nm} = 2\pi^2 \gamma k^2 \, |a_{\mathbf{k}}|^2 , \tag{7}$$

where $\mathbf{k} = (L/2\pi)\mathbf{q}$, $k^2 = n^2 + m^2$; the sum in (7) runs over n and m such that $n^2 + m^2 > 0$. The average of $\tilde{\Phi}_{nm}$ can be easily calculated:

$$\left\langle \tilde{\Phi}_{nm} \right\rangle = \frac{\int\limits_0^{+\infty} \tilde{\Phi}_{nm} e^{-\tilde{\Phi}_{nm}/T} d\, |a_{\mathbf{k}}|}{\int\limits_0^{+\infty} e^{-\tilde{\Phi}_{nm}/T} d\, |a_{\mathbf{k}}|} = \frac{T}{2}. \tag{8}$$

Taking the average of (7) with due regard for (8) we estimate the average squared amplitudes $\left\langle |a_{\mathbf{k}}|^2 \right\rangle = T/4\pi^2\gamma k^2$, $\left\langle |a_{\mathbf{q}}|^2 \right\rangle = T/\gamma q^2 L^2$, and variance of $\xi(x,\, y)$,

$$D[\xi(x,\, y)] \equiv \left\langle \xi^2(x,\, y) \right\rangle = \sum_{n,\, m} \left\langle |a_{\mathbf{k}}|^2 \right\rangle$$

$$= \frac{T}{4\pi^2\gamma} \sum_{n,\, m} \frac{1}{k^2} \simeq \frac{1}{2} \sum_{k=1}^{N_{\max}\sqrt{3}} S_k,$$

where

$$S_k = \frac{T}{\pi k \gamma} = \frac{2T}{Lq\gamma}, \tag{9}$$

and $(1/2)S_k$ is the average squared Fourier amplitude of the fluctuation mode with the wave number $q = 2\pi k/L$. Obviously, estimate (9) for a planar interface can be applied to a large cluster in the short-wavelength limit ($R,\, k \gg 1$). However, a comparison with a similar capillary wave theory for a spherical cluster[8] shows that there is little difference in spectral amplitudes even for moderate k. This agrees with universal behavior (5). Since the variance of surface particles position $D[P(\varphi)] = (1/2) \sum\limits_{k=1}^{k_{\max}} (\alpha_k^2 + \beta_k^2)$, we can compare (9) with spectral amplitudes calculated from simulation data. Figures 4(a) and (b) demonstrate a qualitative agreement: the quantity $T/\pi\gamma$ is close to the average of kS_k calculated from the MD data. The deviation of kS_k from $T/\pi\gamma$ can be accounted for by mode coupling or possible dependence $\gamma(\mathbf{q})$; note that (9) was derived in the approximation of independent modes and constant γ.

The maximum number $N_{\max}$ can be crudely estimated from the following considerations. The minimum wavelength is usually set to the interparticle distance. However, this is true if only an additional condition $|\nabla\xi(x,\,y)|^2 < 1$ is satisfied. Note that the integrand in (6) is the linear term of an expansion, which is valid under the same condition. This linearity condition proves to be the strongest one and, therefore, it defines $N_{\max}$. It also implies that the shortest-wavelength fluctuations satisfying the opposite condition, $|\nabla\xi(x,\,y)|^2 > 1$, are assigned to virtual chains, which are excluded from the present analysis. We assume that the modes up to the number $N_{\max}$ are linear and independent; above this number, their amplitudes are set to zero. Thus, we substitute a smoothly decreasing spectral distribution by the step function. The limiting condition

$$|\nabla\xi(x,\,y)|^2 \sim \left\langle\, |\nabla\xi(x,\,y)|^2 \right\rangle$$
$$= \sum_{\mathbf{q}} q^2 \left\langle |a_{\mathbf{q}}|^2 \right\rangle = \frac{4TN_{\max}^2}{\gamma L^2} = 1$$

yields $N_{\max} = (L/2)\sqrt{\gamma/T}$. Since $\sum\limits_{k=1}^{N_{\max}\sqrt{3}} \frac{1}{k} \simeq \ln\left(N_{\max}\sqrt{3}\right)$, we obtain

$$D[\xi(x,\,y)] \simeq \frac{T}{2\pi\gamma}\ln(N_{\max}\sqrt{3})$$
$$= \frac{T}{2\pi\gamma}\ln\left(\frac{L}{2}\sqrt{\frac{3\gamma}{T}}\right). \qquad (10)$$

Note that variance (10), which defines the interface width, *diverges* as $\ln L$, the logarithm being temperature dependent. It includes no adjustable parameters, in particular, the intrinsic interface width. At the same time, the average excess surface per unit surface area is finite and independent on L: $\langle\Delta A\rangle / L^2 = \langle\Phi\rangle / \gamma L^2 = (1/2)\sum\limits_{n,\,m} q^2 \left\langle |a_{\mathbf{k}}|^2 \right\rangle = 1/2$. This conclusion agrees with the existence of asymptotic value of $g_s g^{-2/3}$ (Fig. 2).

We can estimate the theoretical variance of cluster surface, σ_{th}^2, on the basis of Eq. (10) if we set $q = k/R = 2\pi k/L$, i.e., $L/2 = \pi R = \pi r_\ell g^{1/3}$. Hence, $N_{\max} = \pi r_\ell g^{1/3}\sqrt{\gamma/T}$ and

$$\sigma_{th}^2 = \frac{T}{2\pi\gamma}\ln\left(\Lambda\sqrt{3}\right), \quad \Lambda = \pi r_\ell g^{1/3}\sqrt{\frac{\gamma}{T}} \qquad (11)$$

diverges as $\ln g$. It is noteworthy that the calculation of $\sum\limits_{k=1}^{k_\infty} S_k \simeq \int\limits_1^{k_\infty} S_k\, dk$ with "empirical" S_k (5) leads to the same type of divergence.

The logarithm in (11) decreases as the temperature increases. The maximum wave number is $q_{\max} = N_{\max}/R = \pi\sqrt{\gamma/T}$, therefore, $q_{\max}\sqrt{\left\langle |a_{\mathbf{k}}|^2 \right\rangle} = 1/2N_{\max} \ll 1$ if $N_{\max} \gg 1$ i.e., even for the shortest wavelength the rms mode amplitude is much smaller than respective wavelength. Figure 3 justifies this conclusion. Also, the mode curvature $q_{\max}^2\sqrt{\left\langle |a_{\mathbf{k}}|^2 \right\rangle} = 1/2R \ll 1$ for $R \gg 1$. Hence, it is necessary to take the size correction to surface tension γ in (6) into account only for small clusters with $g < 200$, whose work of formation is not described by the classical liquid drop model (see Ref.[25]).

In addition to the variance calculated using spectral amplitudes based on the MD simulation data, $\sigma_s^2 = (1/2)\sum\limits_{k=1}^{k_{\max}} S_k$, we can introduce a direct estimate

$$\sigma_R^2 = \left\langle \frac{1}{g_s'}\sum_{j=1}^{g_s'} r_j^2 - \left(\frac{1}{g_s'}\sum_{j=1}^{g_s'} r_j\right)^2 \right\rangle,$$

where g_s' is the current number of surface particles; the sum runs over surface particles; angular brackets designate the average over all cluster configurations and cluster sizes in the vicinity of the selected value.

The surface variance can also be determined from a particle density distribution averaged over cluster configurations or time

$$\rho(r) = \frac{1}{4\pi r^2}\frac{dN}{dr}, \qquad (12)$$

where $N(r)$ is the averaged number of internal and surface particles within the sphere of radius r, whose center is situated in the cluster center of mass. For the model of a sharp density change discussed in Sec. III, the local density at distance r from the cluster center of mass is n_ℓ if the cluster instantaneous boundary marked by selected surface particles lies at the distance larger than r; otherwise, it is equal to zero. Therefore, the probability that a point at the distance ζ from the equimolar surface lies outside the cluster is $1 - \rho(\zeta)/n_\ell$, where $\zeta = r - R$, $\rho(-\infty) = n_\ell$, and the cluster is assumed to be sufficiently large. We can define the variance of a random quantity

$$\sigma_\rho^2 = -\frac{1}{n_\ell}\int\limits_{-\infty}^{+\infty}\frac{d\rho}{d\zeta}\,\zeta^2\,d\zeta - \left(\frac{1}{n_\ell}\int\limits_{-\infty}^{+\infty}\frac{d\rho}{d\zeta}\,\zeta\,d\zeta\right)^2, \qquad (13)$$

where $-(1/n_\ell)(d\rho/d\zeta)$ is a normalized distribution function, which characterizes the interface width. Integration by parts of (13) yields

$$\sigma_\rho^2 = \lim_{z\to-\infty}\left[z^2 + \frac{2}{n_\ell}\int\limits_z^\infty \zeta\rho(\zeta)\,d\zeta \right.$$
$$\left. - \left(z + \frac{1}{n_\ell}\int\limits_z^\infty \rho(\zeta)\,d\zeta\right)^2\right]. \qquad (14)$$

Note that definition (14) is free of any model assumption on the analytical form of $\rho(\zeta)$ and can be evaluated numerically.

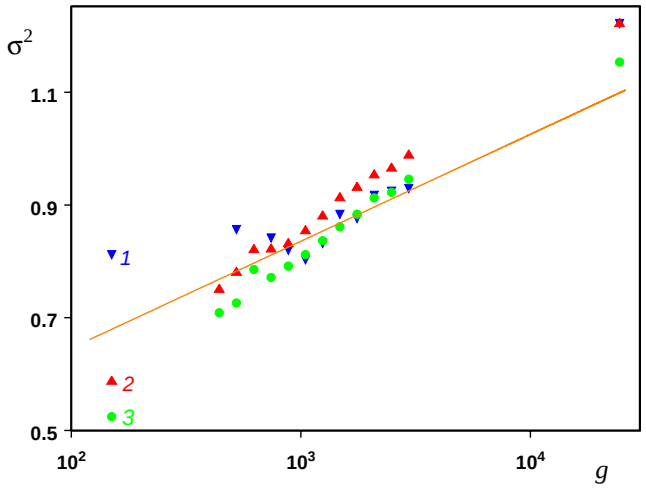

FIG. 6: Surface variance as a function of cluster size; symbols are variances calculated from MD simulation: σ_ρ^2 (1), σ_R^2 (2), σ_s^2 (3); the line represents theoretical estimate (11); $T = 0.75$.

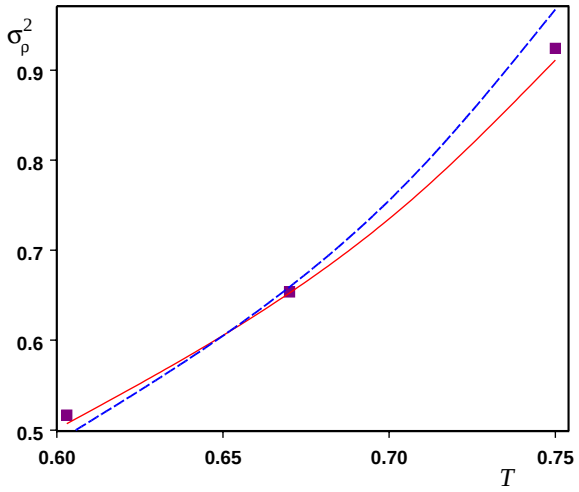

FIG. 7: Temperature dependence of the surface variance for $g = 2482$. Symbols are σ_ρ^2 calculated from the MD simulation; solid line represents estimate (11) and the dashed line represents (15).

One could expect that $\sigma_{th}^2 = \sigma_s^2 = \sigma_R^2 = \sigma_\rho^2$ in the limit of zero interparticle distance. In fact, Fig. 6 shows a satisfactory agreement between these quantities in a wide range of cluster sizes from $g = 150$ to 24450. The deviation of σ_ρ from estimate (11) at small g is connected with the fact that the cluster particle density is no longer constant. The agreement between σ_s^2, σ_R^2, and σ_ρ^2 in Fig. 6 indicates the correctness of the S_k calculation.

The logarithm Λ in (11) can be represented as a ratio of the maximum and minimum wavelengths, $\lambda_{\max} = \pi R = \pi r_\ell g^{1/3}$ and $\lambda_{\min} = \sqrt{T/\gamma}$, respectively. The latter must be larger than the interparticle distance: $\lambda_{\min} > 1$. This limitation was ignored in the deduction of (11). If we set $\lambda_{\min} = 1$, we obtain the variance with a temperature-independent logarithm

$$\sigma_0^2 = \frac{T}{2\pi\gamma} \ln\left(\pi r_\ell g^{1/3}\sqrt{3}\right). \qquad (15)$$

The temperature dependence of variance (15) defined by the ratio T/γ is stronger than that of (11). Figure 7 shows that dependence (11) agrees better with MD simulation estimate of σ_ρ^2 than (15). In the calculation, we used a linear approximation of the surface tension temperature dependence[22] $\gamma(T) = 1.863 - 1.84T$. At $T > 0.65$, $T/\gamma > 1$ and $\sigma_0 > \sigma_{th}$, which means that the condition of linearity of (6) imposes a stronger limitation on $\lambda_{\min}$ than the condition $\lambda_{\min} > 1$. For $g = 3000$, the ratio $\sigma_\rho^2(0.75)/\sigma_\rho^2(0.67) = 1.34$ estimated from the MD simulation agrees better with the theoretical estimate $\sigma_{th}^2(0.75)/\sigma_{th}^2(0.67) = 1.388$ than $\sigma_0^2(0.75)/\sigma_0^2(0.67) = 1.461$, which is in a qualitative agreement with Fig. 5.

V. FREQUENCY FOURIER SPECTRUM

We will consider now the frequency Fourier spectrum of cluster surface fluctuations corresponding to individual cluster evolutions. Since the second mode spectral amplitude is most pronounced, it is convenient to select the instantaneous quantity $\tilde{S}_2(t) = \langle \alpha_2^2 + \beta_2^2 \rangle_{\psi_1,\psi_2}$, which is *not averaged* over configurations of individual clusters, i.e., over the time, to calculate the Fourier transform $G(\omega)$ of $\tilde{S}_2(t)$:

$$G(\omega) \equiv \left\langle |S_\omega|^2 \right\rangle, \qquad S_\omega = (2/\theta) \int_0^\theta \tilde{S}_2(t') \exp(-i\omega t')\, dt', \qquad (16)$$

where $\omega = 2\pi k/\theta$ is the frequency, $k = 1, 2, \ldots$, the inverse transform is

$$\tilde{S}_2(t) = \mathrm{Re}\, S_{\omega=0} + \sum_{k=1}^{\theta/2\tau_\omega} \mathrm{Re}\, S_\omega \cos\omega t - \sum_{k=1}^{\theta/2\tau_\omega} \mathrm{Im} S_\omega \sin\omega t,$$

the angular brackets designate the average over all runs, and $\tau_\omega = 25$ is the time sampling interval. The frequency spectrum was calculated for $T = 0.75$ using the method similar to that discussed in Ref.[20] but unlike that method the average was taken over different runs rather than the time. Successive positions of surface particles during the sampling time $\theta = 1600$, which corresponded to g decreasing from 2000 to 1000, were analyzed numerically for each run of 18 stored. First, the trend was removed from the sample and then the Fourier transform was calculated and averaged over all runs. This averaging makes estimate (16) consistent. Calculation results are shown in Fig. 8. The frequency spectrum is indicative of the

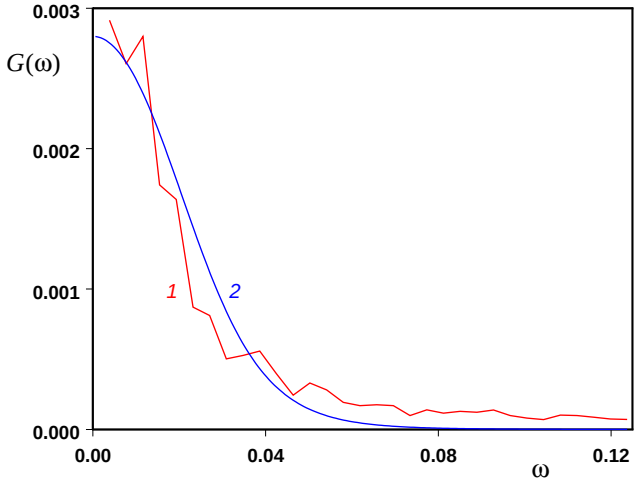

FIG. 8: Frequency Fourier spectrum of cluster surface fluctuations calculated from MD simulation data (1) and theoretical estimate [Eq. (17)] (2).

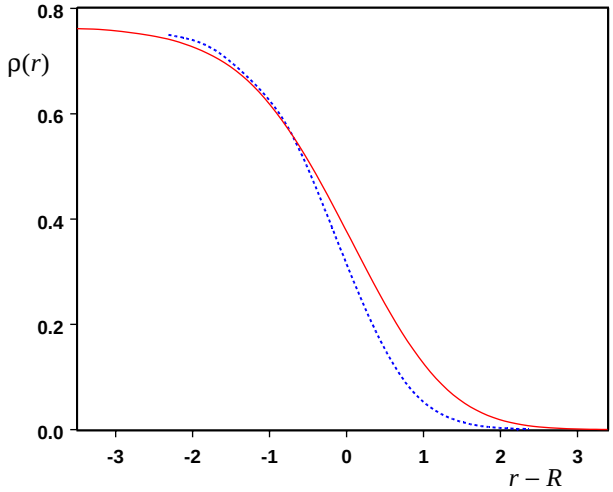

FIG. 9: Particle density distributions for cluster size $g = 150$ (dashed line) and 24450 (solid line); $T = 0.75$.

overdamped dynamic behavior of the cluster surface.

To interpret the form of $G(\omega)$, we consider white-noise-driven forced vibrations of a harmonic oscillator with the eigenfrequency ω_2 and damping factor ν_2. Since the Fourier transform is taken of $\tilde{S}_2$, which is proportional to the time dependence of squared oscillation coordinate, both ω_2 and ν_2 are doubled, and

$$G(\omega) = \frac{C}{[(\omega^2 - 4\omega_2^2)^2 + 4\omega^2\nu_2^2]^2}, \qquad (17)$$

where C is some constant, $\omega_2^2 = 32\pi\gamma_{\rm dim}/3Mg$ corresponds to the eigenfrequency of $Y_{2m}(\Omega)$ mode of liquid droplet capillary oscillations; $\nu_2 = 8\eta/Mn_\ell R^2 = 32\pi\eta r_\ell/3Mg^{2/3}$ is the damping factor for capillary waves, and η is the shear viscosity. Quantities ω_2 and ν_2 are written here in conventional units ($\gamma_{\rm dim}$ is the dimensional surface tension); if η is expressed in units $a^{-2}\sqrt{M\varepsilon/24}$ then dimensionless quantities are $\omega_2^2 = 4\pi\gamma/9g$ and $\nu_2 = 4\pi\eta r_\ell/9g^{2/3}$.

For the average cluster size $g = 1500$, $\omega_2 = 0.0212$, and the MD data spectrum is best fitted by $C = 2.8\times10^{-3}\omega_2^8$ and $\nu_2 = \sqrt{3}\omega_2$ (Fig. 8). In the MD simulation study for the Lennard-Jones fluid[27], the shear viscosity was estimated as $\eta = 11.21$ for conditions compatible with those of the present study. This leads to $\nu_2 = 0.0812 = 3.83\omega_2$, which is 2.2 times higher than the above-mentioned best-fit value. This deviation may arise from the inapplicability of the classical hydrodynamics expression for ν_2; the linear response theory is more adequate for thermocapillary oscillations and leads to a different result[14].

Hence, both the MD simulation result and model considerations are indicative of the fact that the cluster is in the overdamped regime, and *no capillary waves* propagate on its surface. One can treat capillary waves if $\omega_2 > \nu_2$. Since $\omega_2 \sim g^{-1/2}$, $\nu_2 \sim g^{-2/3}$, $\omega_2/\nu_2 = (3g^{1/6}/2\eta r_\ell)(\gamma/\pi)^{1/2} \sim g^{1/6}$; whence $\omega_2/\nu_2 > 1$ at $g > g_w = (2\eta r_\ell/3)^6\,(\pi/\gamma)^3$. For the best-fit value of η mentioned above, we obtain $g \gtrsim 10^5$, i.e. capillary waves can propagate only on the surface of a macroscopic droplet. We treated above the lowest mode $Y_{2m}(\Omega)$. For higher modes with $l > 2$, the boundary of the capillary wave propagation region is even higher. In fact, since we have the eigenfrequency $\omega_l^2 = \pi\gamma l(l-1)(l+2)/18g$ and damping factor $\nu_l = \pi\eta r_\ell l^2/9g^{2/3}$, we obtain the limitation

$$g^{1/3} > g_w^{1/3} = \frac{2\pi}{9}\,\frac{l^3}{(l-1)(l+2)}\,\frac{\eta^2 r_\ell^2}{\gamma}, \qquad (18)$$

from which it follows that $g_w \to \infty$ as $l \to \infty$. It also follows from (18) that the minimum wavelength of capillary waves on the surface of a large cluster is $\lambda_b = 4\pi^2\eta^2 r_\ell^3/9\gamma \sim 10^2$, which is not a microscopic scale. This quantity defines a boundary between the capillary wave and overdamped regimes; the latter regime takes place for wavelengths smaller than λ_b. Therefore, the wavelength λ_b is always much larger than the minimum wavelength of overdamped fluctuations $\lambda_{\rm min}$. The estimate of λ_b for clusters agrees with a similar one for a planar interface[28]. This leads us to the conclusion that *microscopic* capillary waves do not exist.

VI. AVERAGE DENSITY DISTRIBUTION

It was shown in Sec. IV that the independent mode approximation, although it is rather rough, reproduces satisfactory main features of surface fluctuations. It is of interest to investigate the form of the average cluster density distribution function (12) in this approximation. Figure 9 shows the density distribution for two clusters sizes, which are different by two orders of magnitude. In

spite of a noticeable interface width variation, the form of distributions is similar.

Since the position of the surface is a sum of a great number of independent fluctuation modes and the contribution from each mode is small, then, according to the central limit theorem, the distribution of $-(1/n_\ell)(d\rho/d\zeta)$ is normal. Therefore, $\rho(\zeta)$ is given by the error function

$$\rho(\zeta) = \rho_{\rm erf}(\zeta) = \frac{n_\ell}{2}\left[1 - {\rm erf}\left(\frac{\sqrt{\pi}}{d}\zeta\right)\right], \qquad {\rm erf}(\xi) = \frac{2}{\sqrt{\pi}}\int_0^\xi \exp(-t^2)\,dt, \tag{19}$$

where $d = -n_\ell/\rho'(0)$ can be called the interface width.

Instead, it follows from the van der Waals theory that $\rho(\zeta)$ must have the form of hyperbolic tangent (see, e.g., Ref.[29]):

$$\rho(\zeta) = \rho_{\tanh}(\zeta) = \frac{n_\ell}{2}\left[1 - \tanh\left(\frac{2\zeta}{d}\right)\right] \tag{20}$$

with the same interface width. This parameter defines the density distribution variances, which are evaluated using Eq. (13): $\sigma^2_{\rm erf} = d^2/2\pi$ for distribution (19) and $\sigma^2_{\tanh} = \pi^2 d^2/48$ for (20). Note that for the error function, the above-mentioned interface width definition $d = \sigma_{\rm erf}\sqrt{2\pi}$ is not much different from the statistical definition of the normal distribution width $3\sigma_{\rm erf}$.

To decide which theoretical distribution matches better the MD simulation data, $\rho(\zeta)$ was calculated for a cluster size range $2400 < g < 3200$. Since only the asymptotic behavior of functions (19) and (20) at $\zeta \to \pm\infty$ is different, we use the quantity

$$\Delta(\zeta) = \frac{|\rho_{\rm erf}(\zeta) - \rho(\zeta)|}{\rho(\zeta)} + \frac{|\rho(\zeta) - \rho_{\rm erf}(\zeta)|}{n_\ell - \rho(\zeta)} \tag{21}$$

to evaluate the deviation of the MD simulation dependence $\rho(\zeta)$ from $\rho_{\rm erf}(\zeta)$ and a similar quantity with $\rho_{\rm erf}(\zeta)$ substituted for $\rho_{\tanh}(\zeta)$, for the deviation from $\rho_{\tanh}(\zeta)$. Quantity (21) is most sensitive to the deviations at $|\zeta| > 1$ because $\rho(\zeta) \to n_\ell$ at $\zeta \to -\infty$ and $\rho(\zeta) \to 0$ at $\zeta \to +\infty$. We used the value $n_\ell = 0.762$ characteristic of the density of internal particles. Figure 10 shows the function $\Delta(\zeta)$ calculated for both theoretical profiles with the width parameter $d = 2.423$ calculated from a direct MD estimation of $\rho(\zeta)$ (solid symbols) and the values of this parameter that provide the best fit of $\rho_{\rm erf}(\zeta)$ and $\rho_{\tanh}(\zeta)$ to $\rho(\zeta)$, $d = 2.336$ and 2.192, respectively (open symbols). For $\rho_{\tanh}(\zeta)$, the deviation is significantly greater than for $\rho_{\rm erf}(\zeta)$ in both versions of the calculation. The density distribution variance $\sigma^2_{\rm erf} = 0.935$ estimated at $d = 2.336$ agrees much better with $\sigma^2_\rho = 0.934$ than the variance of alternative density profile $\sigma^2_{\tanh} = 1.208$. A better adaptability of profile (19) was noted in Refs.[8,18,19].

Therefore, the error function profile (19) is more adequate for the interpretation of the MD simulation data, which confirms the model of cluster surface fluctuations discussed in this study.

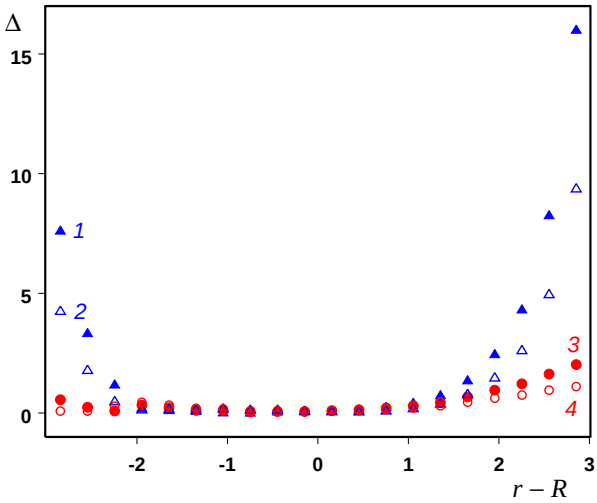

FIG. 10: Deviation of cluster density profile from theoretical prediction [Eq. (20)] (1), (2) and [Eq. (19)] (3), (4) calculated for d estimated from MD simulation data (1), (3) and for best-fit values of d (2), (4).

VII. CONCLUSIONS

We showed that cluster particles are virtually divided in three groups, the internal particles, surface particles, and virtual chains. Such a classification is based on definition (2). Fairly resolvable modes of the distribution over a number of bonds are indicative of the fact that the surface and internal particles form the groups of particles with entirely different properties. Surface particles can be treated as a surface phase that lies between the liquid and vapor phases. It was discussed by Gibbs and is sometimes called a "surface azeotrope"[2].

The MD simulation data led us to the model of a nonspherical cluster boundary with the abrupt change of density from bulk liquid to a vapor one. This boundary is an instantaneous conceptual surface that passes through the surface particles. Deviations of this surface from spherical form arise from thermal fluctuations. We characterized these fluctuations by their Fourier spectra in wave number and frequency. Wave-number spectra calculated for different cluster sizes show universal behavior, which within the accuracy of this simulation is not affected by the variation of different system parameters, e.g., the vapor density. The scaled spectral amplitudes are approximated by function (5), whose numerical constants are defined solely by the temperature. The wave-number dependence of spectral amplitudes therefore has the form $1/q - \text{const}$, i.e., it decreases faster than $1/q$. We did not find a relevant theory in the literature that could account for such dependence and the temperature dependence of modes with different k (Fig. 5). Possible reasons for such behavior could be the coupling of fluctuation modes or the wave-number dependence of the surface tension.

Surface fluctuation spectra obtained in the MD sim-

ulation can be qualitatively interpreted using a simple version of the fluctuation theory [work of fluctuation formation (6)] with an additional wave-number cutoff that provides mode linearity. Although the theory yields just a crude description of the wave-number dependence of spectral amplitudes, the estimate of the cluster surface variance as a function of size and temperature matches respective variance dependences calculated on the basis of MD simulation spectral amplitudes, positions of the surface particles, and the average cluster density distribution. All dependences diverge with the cluster size as $\ln g$. Note that estimate (11) derived in this study agrees better with the variance temperature dependence of the MD simulation than a conventional estimate with the temperature-independent logarithm.

The frequency spectrum of amplitude S_2 points to the overdamped dynamic system behavior. The estimate based on the damped oscillator model leads to the conclusion that thermocapillary waves can propagate only on the surface of macroscopic drops; the term "capillary waves" is inapplicable for clusters or, generally speaking, small simulation ensembles. This conclusion is valid not only for the Lennard-Jones system but for other substances, as one can easily verify using condition (18), which follows from macroscopic hydrodynamics.

As we showed in this study, the wave-number dependence of spectral amplitudes deviates from $1/q$. This deviation is important even if it is small because the integral of $1/q$ that defines the surface variance (or interface width) diverges on both limits. Based on the independent mode approximation, it was shown in Ref.[8] that all average amplitudes of cluster surface spherical modes $Y_{lm}(\Omega)$ have the same temperature dependence, which contradicts Fig. 5. The variance size dependence[8] estimated with the number of surface modes $N_{\max}$ would lie somewhat lower and parallel to the solid line in Fig. 6, i.e., the difference in the integral characteristic of a spherical and planar interface is minor. Apparently mode coupling has no effect on the average density profile: the error function, which follows from independent mode approximation, reproduces the cluster density profile more adequately.

According to the analytical estimates of Sec. IV the surface perturbed by thermal fluctuations or the actual surface must be on the average 1.5 times larger than the unperturbed one. Therefore, the quantity γ in (6) should be substituted for some coupling constant or the "internal" surface tension $\gamma_0 < \gamma$. This would lead to the increase of S_k and slope of the curve in Fig. 6. Fluctuations with the wavelength $\lambda < \lambda_b$ must have the same order of magnitude as capillary waves with $\lambda > \lambda_b$. If the minimum wavelength for a macroscopic system was estimated as λ_b then, since $\lambda_{\min} \ll \lambda_b$, the value of $N_{\max}$ and therefore of ΔA would be underestimated by orders of magnitude. This would lead to $\gamma_0 = \gamma$, which seems not to be true. Hence, it is the short-wavelength range that is responsible for the difference between γ and γ_0; this range should not be neglected even for a macroscopic system. To establish the relation between γ and γ_0, one needs an exact description of the Fourier coefficients distribution over $\mathbf{q}$. In view of the foregoing, the development of a theory (e.g., a relevant approximation of the density functional theory) that would allow for possible dependence $\gamma_0(\mathbf{q})$, mode coupling, and wavelength cutoff at the interparticle distance is urgent.

One can expect that thermal fluctuations spectrum would retain the form (5) for a planar liquid–vapor interface. It is therefore of interest to check this prediction. Since a planar interface is anisotropic, it could be possible to calculate the quantity $\left\langle |a_{\mathbf{q}}|^2 \right\rangle$ as a function of $\mathbf{q}$, which is a more detailed spectral characteristic than S_k, although this would require more computational efforts.

* Electronic address: dmrzhu@yandex.ru

[1] J. W. Gibbs, in *The Collected Works of J. Willard Gibbs* (Yale University Press, New Haven, 1948), Vols. 1 and 2.
[2] J. Rowlinson and B. Widom, *Molecular Theory of Capillarity* (Clarendon Press, Oxford, 1982).
[3] J. Frenkel, *Kinetic Theory of Liquids* (Dover, New York, 1955).
[4] F. P. Buff, R. A. Lovett, and F. H. Stillinger, Phys. Rev. Lett. **15**, 621 (1965).
[5] J. D. Weeks, J. Chem. Phys. **67**, 3106 (1977).
[6] J. V. Sengers and J. M. J. van Leeuwen, Phys. Rev. A **39**, 6346 (1989).
[7] J. Meunier, J. Phys. (Paris) **48**, 1819 (1987).
[8] N. Pavloff and C. Schmit, Phys. Rev. B **58**, 4942 (1998).
[9] S. Fisk and B. Widom, J. Chem. Phys. **50**, 3219 (1969).
[10] M. Napiórkowski and S. Dietrich, Phys. Rev. E **47**, 1836 (1993).
[11] K. R. Mecke and S. Dietrich, Phys. Rev. E **59**, 6766 (1999).
[12] B. M. Ocko, X. Z. Wu, E. B. Sirota, S. K. Sinha, and M. Deutsch, Phys. Rev. Lett. **72**, 242 (1994).
[13] T. Seydel, A. Madsen, M. Tolan, G. Grübel, and W. Press, Phys. Rev. B **63**, 073409 (2001).
[14] A. Madsen, T. Seydel, M. Sprung, C. Gutt, M. Tolan, and G. Grübel, Phys. Rev. Lett. **92**, 096104 (2004).
[15] A. Datta, S. Kundu, M. K. Sanyal, J. Daillant, D. Luzet, C. Blot, and B. Struth, Phys. Rev. E **71**, 041604 (2005).
[16] J. W. Schmidt, Phys. Rev. A **38**, 567 (1988).
[17] P. Cicuta, A. Vailati, and M. Giglio, Phys. Rev. E **62**, 4920 (2000).
[18] S. W. Sides, G. S. Grest, and M.-D. Lacasse, Phys. Rev. E **60**, 6708 (1999).
[19] A. E. Ismail, G. S. Grest, and M. J. Stevens, J. Chem. Phys. **125**, 014702 (2006).
[20] D. I. Zhukhovitskii, J. Chem Phys. **103**, 9401 (1995).
[21] A. Rytkönen, S. Valkealahti, and M. Manninen, J. Chem. Phys. **108**, 5826 (1998).
[22] A. E. van Giessen and E. M. Blokhuis, J. Chem Phys. **116**, 302 (2002).

[23] F. H. Stillinger, Jr., J. Chem. Phys. **38**, 1486 (1963).
[24] D. I. Zhukhovitskii, J. Exp. Theor. Phys. **94**, 336 (2002).
[25] D. I. Zhukhovitskii, J. Chem. Phys. **110**, 7770 (1999).
[26] S. I. Anisimov, D. O. Dunikov, V. V. Zhakhovskii, and S. P. Malyshenko, J. Chem. Phys. **110**, 8722 (1999).
[27] K. Meier, A. Laesecke, and S. Kabelac, J. Chem. Phys. **121**, 3671 (2004).
[28] G. Sh. Boltachev and V. G. Baidakov, Colloid Journal **68**, 26 (2006).
[29] V. G. Baidakov, S. P. Protsenko, G. G. Chernykh, and G. Sh. Boltachev, Phys. Rev. E **65**, 041601 (2002).